Sensors

Deutsche Ausgabe: DOI: 10.1002/ange.201504027
Internationale Ausgabe: DOI: 10.1002/anie.201504027

Plasmonic Colloidosomes as Three-Dimensional SERS Platforms with Enhanced Surface Area for Multiphase Sub-Microliter Toxin Sensing**

*Gia Chuong Phan-Quang, Hiang Kwee Lee, In Yee Phang, and Xing Yi Ling**

Abstract: *Colloidosomes are robust microcapsules attractive for molecular sensing because of their characteristic micron size, large specific surface area, and dual-phase stability. However, current colloidosome sensors are limited to qualitative fluorogenic receptor-based detection, which restrict their applicability to a narrow range of molecules. Here, we introduce plasmonic colloidosome constructed from Ag nanocubes as an emulsion-based 3D SERS platform. The colloidosomes exhibit excellent mechanical robustness, flexible size tunability, versatility to merge, and ultrasensitivity in SERS quantitation of food/industrial toxins down to sub-femtomole levels. Using just 0.5 μL of sample volumes, our plasmonic colloidosomes exhibit >3000-fold higher SERS sensitivity over conventional suspension platform. Notably, we demonstrate the first high-throughput multiplex molecular sensing across multiple liquid phases.*

Colloidosomes are three-dimensional (3D) spherical microcapsules formed by the self-assembly of colloidal particles at an emulsion interface, whereby a dispersed liquid is encapsulated within a continuous liquid medium.[1] Typically, a microliter volume of dispersed liquid is emulsified into tens of thousands of micrometer-sized liquid core–solid shell structures with a concurrent hundred-fold enhancement in effective surface area.[1b,2] The versatility choice of their building blocks also allows easy incorporation of unique properties into colloidosome,[3] which enable their wide applicability in controlled delivery and release,[4] and small-volume biphasic catalysis.[5]

One less explored yet greatly attractive application of colloidosomes is their use as miniaturized molecular sensing platforms,[6] owing to their microliter volume, large surface area, and excellent interfacial stability.[7] Previously, fluorescence-based colloidosome sensor has been used to qualitatively detect fructose by embedding colloidosomes with fluorogenic receptors.[6] However, such method provides limited molecular information and also narrows the choice of detectable fluorescent analyte. These limitations can be addressed using "plasmonic colloidosomes" constructed from noble-metal (Ag or Au) nanoparticles which use surface-enhanced Raman scattering (SERS) effect,[8] arising from the intense electromagnetic field upon incident excitation, to provide a highly specific vibrational fingerprint of molecules even at ultratrace concentration.[9]

In addition, the 3D morphology of the plasmonic colloidosomes enables efficient laser interaction because of their high SERS hot spot density across all spatial planes within the laser illumination volume, and also high tolerance toward laser focus misalignment.[9a,10] Colloidosomes also enable direct and simultaneous SERS detection of multiple molecules present in two immiscible phases because of their robust emulsion-based template. Hence, plasmonic colloidosomes can overcome the general drawbacks of current interfacial SERS platforms based on liquid–liquid assembly of two-dimensional (2D) nanoparticle monolayers,[11] such as the latter's under-utilization of laser confocal volume and potential susceptibility to signal fluctuations on thermal/physical agitation.[10] The application of plasmonic colloidosomes in interfacial SERS sensing therefore provides an ideal generic molecular sensor that can greatly facilitate on-site detection of multi-phase samples in food and environmental analysis.

Herein, we demonstrate the fabrication of plasmonic colloidosomes and their application as an emulsion-based 3D SERS platform for the multiplex toxin detection in sub-microliter volumes of both water and organic phases. Our fabrication strategy involves the emulsification of immiscible liquids in the presence of plasmonic Ag nanocubes. We first examine their physical and mechanical properties such as shell thickness, durability, ability to merge and size tunability. We then determine the 3D SERS-active areas of our colloidosomes and subsequently study the single-phase ultratrace and quantitative SERS detection of toxins at sub-femtomolar levels. Our plasmonic colloidosomes are further evaluated for multiplex detection of analytes in the same phase, and also across two immiscible liquid phases. The superiority of our plasmonic colloidosomes will also be demonstrated over conventional suspension SERS platform.

We employ Ag nanocubes as the building blocks for the construction of plasmonic colloidosomes because of their strong localized surface plasmons upon excitation by visible light,[9a] and also their well-defined tips and edges that produce intense electric field for SERS enhancement.[12] Ag nanocubes with excellent monodispersity of about 120 nm (see Figure S1 in the Supporting Information),[13] are func-

[*] G. C. Phan-Quang, H. K. Lee, Prof. X. Y. Ling
Division of Chemistry and Biological Chemistry
School of Physical and Mathematical Sciences
Nanyang Technological University
21 Nanyang Link, Singapore 637371 (Singapore)
E-mail: xyling@ntu.edu.sg
H. K. Lee, Dr. I. Y. Phang
Institute of Materials Research and Engineering
Agency for Science, Technology and Research (A*STAR)
3 Research Link, Singapore 117602 (Singapore)

[**] X.Y.L. thanks Singapore National Research Foundation (grant number NRF-NRFF2012-04) for support. H.K.L. thanks the A*STAR graduate scholarship from A*STAR, Singapore. SERS = surface-enhanced Raman spectroscopy.

Supporting information for this article is available on the WWW under http://dx.doi.org/10.1002/anie.201504027.

tionalized with perfluorodecanethiol (PFDT) to impart omniphobicity[14] essential for stabilizing our water-in-oil colloidosomes.[2d]

Plasmonic colloidosomes are prepared by simply shaking a mixture of 0.5 μL dispersed water in 200 μL continuous decane in the presence of 0.20 mg PFDT-functionalized Ag nanocubes (Figure 1 A). The resulting spherical water-in-decane colloidosomes have average diameter of (40 ± 10) μm (Figure 1 B,E) and possess rough shells composed of Ag nanocube clusters (Figure S2). Based on the hollow frames of dried colloidosomes (Figure 1 I–J), we approximate the shell thickness at (1560 ± 360) nm, which is equivalent to (13 ± 3) layers of Ag nanocubes (Figure S3). These closely packed clusters of Ag nanocubes are essential in generating intense electromagnetic field for Raman enhancement because of plasmonic coupling across all spatial directions (x, y, and z).[9a] Together with the formation of more than 10^4 colloidosomes and more than 26-fold enhancement in the surface area compared to the original water droplet (see the Supporting Information), plasmonic colloidosomes provide an ultrasensitive and large-area SERS platform for ultratrace toxin detection.

Plasmonic colloidosomes also demonstrate size-tunability via the manipulation of water/Ag nanocubes (abbreviated as water/Ag) ratio during emulsification. As the water/Ag ratio is increased from 2.5 to 12.5 μL mg^{-1}, the diameter of the colloidosomes increases linearly from the initial 40 to about 200 μm (Figure 1 B–D, E–H; Figure S4). In contrast, the colloidosomes' size is not influenced by decane volume (Figure S5). The linear relationship between the diameter of the colloidosomes and the water/Ag ratio indicates the presence of an optimal Ag nanocube shell thickness to stabilize the water/decane interface, which we further affirm the consistency of the colloidosome shell thickness by SEM imaging (Figure S3). It is therefore evident that our plasmonic colloidosomes are highly versatile in accommodating a diverse range of microliter volumes. Hereupon, we use 40 μm plasmonic colloidosomes fabricated from 2.5 μL mg^{-1} water/Ag ratio for latter discussion, unless otherwise stated, to emphasize the ultralow sample volume required for colloidosome preparation.

We perform x-y and x-z hyperspectral SERS imaging of individual colloidosomes containing methylene blue dye (1 μM) to identify their SERS active area. From the x-y SERS imaging, we observe that the SERS-active regions (brightly lit areas in Figure 2 A–C; Figure S6) of plasmonic colloidosomes exhibit characteristic vibrational modes of methylene blue (Figure S7, Table S1), which resemble the normal Raman spectrum of the same molecule without Ag nanoparticles (Figure S8). The featureless SERS spectrum obtained in the absence of the dye affirms that the observed signals originate from the target analyte and not from the surface ligands or solvent (Figures S7, S9). Using the most intense C=C stretching mode of methylene blue at 1633 cm^{-1}, we observe a strong dependency of the SERS-active areas on the confocal plane of the excitation laser when using a 20× objective lens with about 3.6 μm resolvable resolution (Figure S10). For instance, focusing the laser confocal plane at the top and mid-plane of plasmonic colloidosomes result in strong SERS responses (ca. 4900 counts per second) mainly confined

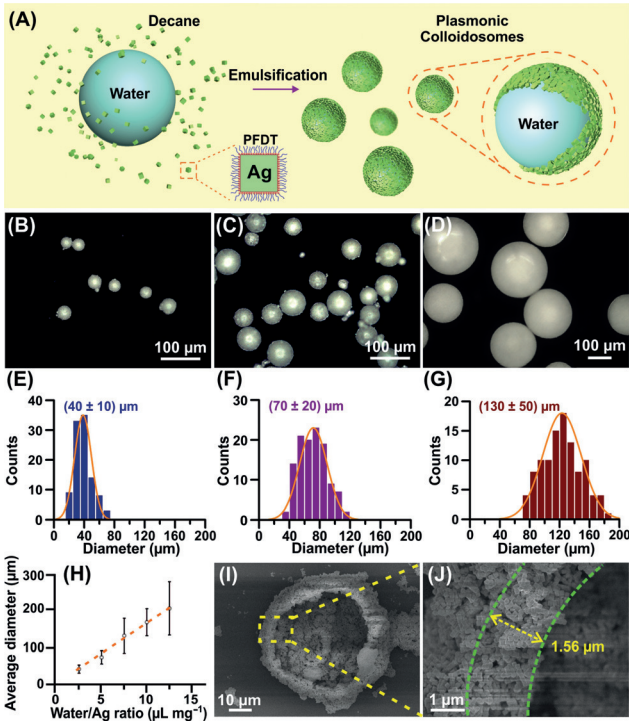

Figure 1. A) Schematic illustrating the formation of plasmonic colloidosomes. Microscopic images of colloidosomes formed using water/Ag ratio of B) 2.5, C) 5.0 and D) 7.5 μL mg^{-1} with (E–G) their corresponding size distributions. H) Correlation of water/Ag ratio during colloidosome formation to their resulting diameters. SEM images of I) a hollow colloidosome shell and the J) magnified segment.

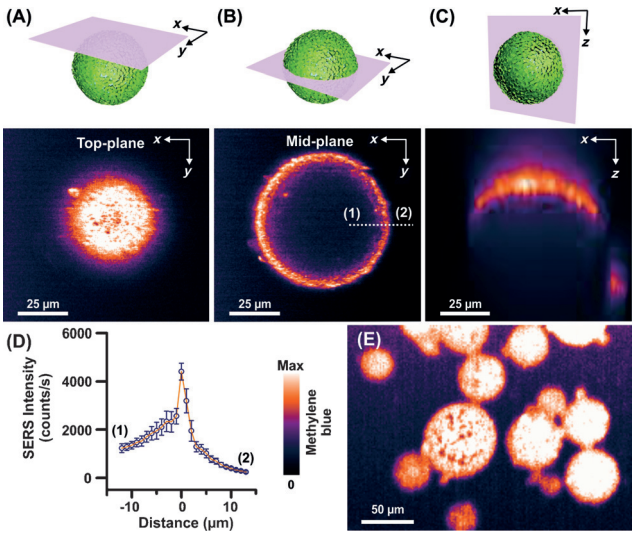

Figure 2. Schematics (top) and corresponding x-y SERS images (bottom) when laser is focused A) on top, and B) at the mid-plane of the colloidosome. C) Schematic (top) and the corresponding x-z SERS image (bottom) image of colloidosome. D) SERS intensity–distance profile along the white dotted line of (B), from (1) to (2). (A–D) uses a 20× objective lens. E) SERS image of colloidosomes using a 4× objective lens. All the colloidosomes contain methylene blue 10^{-6} M and are submerged in decane.

to the top and edge of the colloidosomes (Figure 2A,B,D), respectively. Subsequent *x*-*z* SERS imaging of the plasmonic colloidosomes further exemplifies the localization of strong SERS-activity (ca. 4720 counts per second) to the Ag nanocube shell (Figure 2C; Figure S11).[9a] Collectively, both the *x*-*y* and *x*-*z* SERS images highlight the applicability of the entire colloidosome shell for SERS detection. This is again illustrated using a wide-field 4× objective lens with a larger depth-of-field (Figures S6, S10) where the whole 3D plasmonic shell of colloidosomes shows strong SERS activity (ca. 4000 counts per second), even at attomole level of methylene blue (Figure 2E; see the Supporting Information). Furthermore, consistent SERS activities are observed from colloidosomes of varying sizes and also over an extended storage duration of more than 340 h (Figures S12, S13), highlighting that plasmonic colloidosomes are durable and support reproducible signals for various sample volumes.

The mechanically robust plasmonic colloidosomes also demonstrate excellent versatility by their ability to merge upon re-emulsification to homogenize their encapsulated aqueous content (Figure 3A). When two plasmonic colloidosomes are placed together, each separately contains methylene blue (1 μM) and rhodamine 6G (1 μM), SERS bands unique to methylene blue (456 cm^{-1} and 503 cm^{-1}) and rhodamine 6G (620 cm^{-1}) are observed distinctly in the respective colloidosomes (Figure 3C) with no apparent cross-transfer of the analytes. Upon re-emulsification (Figure 3D), the colloidosomes merge and equally homogenize their encapsulated contents into newly merged colloidosomes (Figure S14), which exhibit a multiplex SERS spectrum, consisting of signals characteristic to both methylene blue and rhodamine 6G at 456 cm^{-1} and 620 cm^{-1}, respectively (Figure 3B,D). Such ability to merge and homogenize aqueous content by re-emulsification is crucial in the field of sensing and microreaction, where additional species such as reactants and spectroscopic reference can be easily added into colloidosomes on demand.

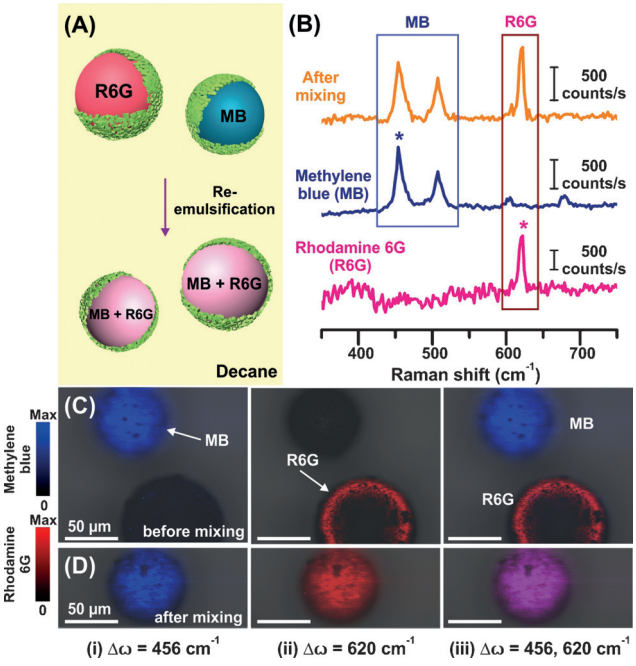

Figure 3. A) Schematic illustration of the merging of colloidosomes. B) SERS spectra for the multiplex detection of methylene blue and rhodamine 6G in a single colloidosome (top), and also individual detection of methylene blue (middle), and rhodamine 6G (bottom) in separate colloidosomes. C) SERS images overlaid with corresponding optical image of two distinct colloidosomes before mixing. D) SERS image overlaid with an optical image of a colloidosome containing both analytes after mixing. The SERS images are color-indexed using blue and red for methylene blue (i; 456 cm^{-1}) and rhodamine 6G (ii; 620 cm^{-1}), respectively. Magenta color in (iii) denotes the presence of both methylene blue and rhodamine 6G in a single colloidosome.

We apply plasmonic colloidosomes for the SERS detection of several industrial toxins,[15] to demonstrate the importance of large 3D SERS-active surfaces as sensitive and reproducible analytical platforms. To fully utilize the 3D SERS area of the colloidosomes for detecting sub-microliter liquid phases, a wide-field 4× objective lens is used for averaging the SERS spectra over a large scan area (1850 μm × 1350 μm) comprising of more than 10^3 closely packed colloidosomes (Figure S6), and analyte concentrations are reported in mole number, respectively. The individual detection of rhodamine 6G in the aqueous phase and coumarin in the organic phase achieves a detection limit of 0.5 and 5 fmol, with the corresponding analytical enhancement factors (AEF) of 2×10^6 and 5×10^7, respectively (Figure 4A, Figure S15–18). This denotes that our plasmonic colloidosome is able to enhance a Raman signal by more than 10^6, in comparison to the signal in the absence of the plasmonic Ag nanocube shell. In addition, our plasmonic colloidosomes also show a 3000-fold superior SERS activity relative to a coumarin-containing decane suspension of the same mass of Ag nanocubes (Figure S19), where the latter only exhibits an analytical enhancement factor of 2×10^4. The general Raman enhancement of $>10^6$ provided by plasmonic colloidosome originates from both the intense and dense SERS hotspot in the closely packed Ag nanocube of the colloidosomes' shells, and also from the large 3D area imparted by plasmonic colloidosomes.

Our colloidosome platform affords linear intensity–concentration relationships for both rhodamine 6G and coumarin, and also other aqueous- or organic-soluble toxins/analytes (Figure 4A; Figures S7, S15, S17, S20, and S23), which directly exemplifies the high signal reproducibility crucial for quantitative analysis, even down to sub-femtomole level of toxins. Furthermore, all the ultratrace detection requires only 0.5 μL of the encapsulated aqueous phase and 5.0 μL of the exterior organic phase, which is advantageous over conventional 2D interfacial SERS techniques that need milliliter volume of liquids.[10] Such sub-microliter volume detection is important in the field of forensic, clinical diagnosis, and toxin detection, especially when analytes are highly toxic/hazardous and/or sample availability is scarce.[16]

The plasmonic colloidosomes also excel in multiplex detection and quantification of toxins simultaneously across a liquid-liquid interface. To demonstrate a triplex interfacial detection, we separately encapsulate malachite green (5 pmol, 9% mol) and rhodamine 6G (0.5 pmol, 1% mol) in plasmonic colloidosomes and mix them in a decane solution

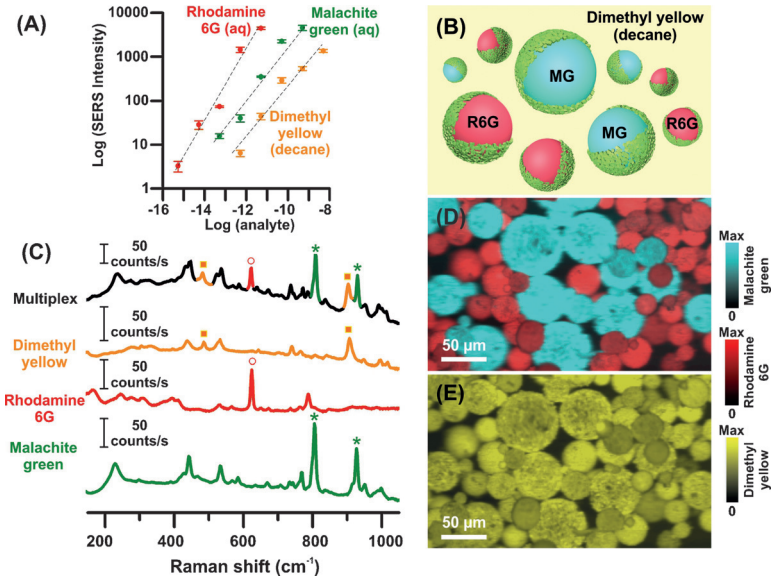

Figure 4. A) SERS intensity at various mole numbers of malachite green, rhodamine 6G, and dimethyl yellow in their individual detection. B) Schematic depicting the "dual-phase tri-analyte" multiplex detection using plasmonic colloidosomes. C) SERS spectra of multiplex detection (black) and also individual detections of malachite green (green), rhodamine 6G (red), and dimethyl yellow (yellow). SERS images of multiplex detection using plasmonic colloidosomes when characteristic bands of D) malachite green (cyan) and rhodamine 6G (red), and also E) dimethyl yellow (yellow) are selected.

containing dimethyl yellow (50 pmol, 90% mol; Figure 4B). The overall multiplex SERS spectrum in Figure 4C exhibits distinguishable fingerprint signals that can be indexed to individual analytes; 808 and 929 cm^{-1} for malachite green, 620 cm^{-1} for rhodamine 6G and 483, 739 and 905 cm^{-1} for dimethyl yellow. When the characteristic SERS band of malachite green at 808 cm^{-1} is selected, only a portion of the colloidosomes (cyan) demonstrate SERS activity (Figure 4D). Likewise, when the SERS band of rhodamine 6G 620 cm^{-1} is highlighted, high SERS activities are observed on the remaining portion of colloidosomes (red; Figure 4D). On the other hand, the selection of SERS band at 905 cm^{-1}, which is unique only to dimethyl yellow in the exterior phase, reveals that all the colloidosomes (yellow) demonstrate SERS responses to the common organic-soluble analyte, (Figure 4E). Most importantly, the intensities of the selected SERS bands of different analytes in the multiplex detection can be quantitatively matched within the standard of deviation of those observed in the individual detection Scheme (Figure S24, see also the Supporting Information). This highlights the ability to quantify both absolute amount and relative percentage of each toxins in a mixture. To the best of our knowledge, this is the first interfacial SERS sensing using a miniaturized "dual-phase tri-analyte" multiplex detection set-up. This is an advancement to existing interfacial SERS methods, which are typically restricted to the determination of relative concentrations between two analytes only, possibly due to signal fluctuations and also relatively larger SERS platform size that is unsuitable for the analysis of additional analyte compartment.[12] It is therefore evident that the excellent mechanical robustness and interfacial stability, large specific 3D SERS-active area, and micron-sized of colloidosomes are all crucial factors in achieving highly-sensitive, miniature SERS platform capable of complex sensing and quantification of multiple analytes and/or liquid phases.

In conclusion, we have constructed size-tunable plasmonic colloidosomes using Ag nanocubes as emulsion-based 3D multiplex SERS sensing platforms for ultralow sample volumes. Our plasmonic colloidosomes are capable of ultratrace detection of both aqueous- and organic-soluble toxins down to sub-femtomole levels, and also quantitative analysis over 5-order of magnitudes, all using just sub-microliter sample volumes. By exploiting the micron-sized plasmonic colloidosomes and their large and reproducible SERS enhancement of more than 10^6-fold, we demonstrate the first "dual-phase tri-analyte" interfacial detection scheme for the high through-put detection and quantification of three analytes across multiple liquid phases simultaneously. The ensemble of benefits of plasmonic colloidosomes enables them as an immensely attractive, miniaturized SERS analytical platform crucial for on-site detection in the field of forensic and also industrial, food and environment safety.

Keywords: colloidosomes · sensors · silver nanoparticles · surface-enhanced Raman scattering · toxin

How to cite: *Angew. Chem. Int. Ed.* **2015**, *54*, 9691–9695
Angew. Chem. **2015**, *127*, 9827–9831

[1] a) H. N. Yow, A. F. Routh, *Soft Matter* **2006**, *2*, 940–949; b) A. D. Dinsmore, M. F. Hsu, M. G. Nikolaides, M. Marquez, A. R. Bausch, D. A. Weitz, *Science* **2002**, *298*, 1006–1009.
[2] a) C. Yuan, B. Zeng, S. Yu, J. Mao, X. Chen, W. Luo, Y. Xu, F.-C. Chang, L. Dai, *R. Soc. Chem. Adv.* **2014**, *4*, 4796–4803; b) O. J. Cayre, P. F. Noble, V. N. Paunov, *J. Mater. Chem.* **2004**, *14*, 3351–3355; c) P. F. Noble, O. J. Cayre, R. G. Alargova, O. D. Velev, V. N. Paunov, *J. Am. Chem. Soc.* **2004**, *126*, 8092–8093; d) F. Leal-Calderon, V. Schmitt, J. Bibette, *Emulsion Science: Basic Principles*, Springer, **2007**; e) T. Bollhorst, S. Shahabi, K. Wörz, C. Petters, R. Dringen, M. Maas, K. Rezwan, *Angew. Chem. Int. Ed.* **2015**, *54*, 118–123; *Angew. Chem.* **2015**, *127*, 120–125.
[3] a) A. San Miguel, J. Scrimgeour, J. E. Curtis, S. H. Behrens, *Soft Matter* **2010**, *6*, 3163–3166; b) S. Zhou, J. Fan, S. S. Datta, M. Guo, X. Guo, D. A. Weitz, *Adv. Funct. Mater.* **2013**, *23*, 5925–5929; c) M. Li, R. L. Harbron, J. V. M. Weaver, B. P. Binks, S. Mann, *Nat. Chem.* **2013**, *5*, 529–536.
[4] S. Li, B. A. Moosa, J. G. Croissant, N. M. Khashab, *Angew. Chem. Int. Ed.* **2015**, *54*, 6804–6808; *Angew. Chem.* **2015**, *127*, 6908–6912.
[5] Z. Wang, M. C. M. van Oers, F. P. J. T. Rutjes, J. C. M. van Hest, *Angew. Chem. Int. Ed.* **2012**, *51*, 10746–10750; *Angew. Chem.* **2012**, *124*, 10904–10908.
[6] X. Shen, C. Xu, K. M. A. Uddin, P.-O. Larsson, L. Ye, *J. Mater. Chem. B* **2013**, *1*, 4612–4618.

[7] a) D. Lee, D. A. Weitz, *Adv. Mater.* **2008**, *20*, 3498 – 3503; b) B. Samanta, D. Patra, C. Subramani, Y. Ofir, G. Yesilbag, A. Sanyal, V. M. Rotello, *Small* **2009**, *5*, 685 – 688.
[8] L. Polavarapu, J. Perez-Juste, Q.-H. Xu, L. M. Liz-Marzan, *J. Mater. Chem. C* **2014**, *2*, 7460 – 7476.
[9] a) H. Ko, S. Singamaneni, V. V. Tsukruk, *Small* **2008**, *4*, 1576 – 1599; b) M. Alba, N. Pazos-Perez, B. Vaz, P. Formentin, M. Tebbe, M. A. Correa-Duarte, P. Granero, J. Ferré-Borrull, R. Alvarez, J. Pallares, A. Fery, A. R. de Lera, L. F. Marsal, R. A. Alvarez-Puebla, *Angew. Chem. Int. Ed.* **2013**, *52*, 6459 – 6463; *Angew. Chem.* **2013**, *125*, 6587 – 6591; c) L. Guerrini, E. Pazos, C. Penas, M. E. Vázquez, J. L. Mascareñas, R. A. Alvarez-Puebla, *J. Am. Chem. Soc.* **2013**, *135*, 10314 – 10317.
[10] Q. Zhang, Y. H. Lee, I. Y. Phang, C. K. Lee, X. Y. Ling, *Small* **2014**, *10*, 2703 – 2711.
[11] a) M. P. Konrad, A. P. Doherty, S. E. J. Bell, *Anal. Chem.* **2013**, *85*, 6783 – 6789; b) K. Zhang, J. Ji, Y. Li, B. Liu, *Anal. Chem.* **2014**, *86*, 6660 – 6665; c) M. P. Cecchini, V. A. Turek, J. Paget, A. A. Kornyshev, J. B. Edel, *Nat. Mater.* **2013**, *12*, 165 – 171; d) K. Kim, H. S. Han, I. Choi, C. Lee, S. Hong, S.-H. Suh, L. P. Lee, T. Kang, *Nat. Commun.* **2013**, *4*, 2182.
[12] H. K. Lee, Y. H. Lee, I. Y. Phang, J. Wei, Y.-E. Miao, T. Liu, X. Y. Ling, *Angew. Chem. Int. Ed.* **2014**, *53*, 5054 – 5058; *Angew. Chem.* **2014**, *126*, 5154 – 5158.
[13] M. Mulvihill, A. Tao, K. Benjauthrit, J. Arnold, P. Yang, *Angew. Chem. Int. Ed.* **2008**, *47*, 6456 – 6460; *Angew. Chem.* **2008**, *120*, 6556 – 6560.
[14] X. Li, H. K. Lee, I. Y. Phang, C. K. Lee, X. Y. Ling, *Anal. Chem.* **2014**, *86*, 10437 – 10444.
[15] S. S. Deshpande, *Handbook of Food Toxicology*, Taylor & Francis, New York, **2002**.
[16] X. Niu, F. Gielen, J. B. Edel, A. J. deMello, *Nat. Chem.* **2011**, *3*, 437 – 442.

Received: May 3, 2015
Published online: June 26, 2015

